Brief Report

Pal power: Demonstration of the functional association of the *Helicobacter pylori* flagellar motor with peptidoglycan-associated lipoprotein (Pal) and its preliminary crystallographic analysis

Xiaotian Zhou[1], Mohammad M. Rahman[1], Sharmin Q. Bonny[1], Yue Xin[1], Nikki Liddelow[2], Mohammad F. Khan[1], Alexandra Tikhomirova[1], Jihane Homman-Ludiye[3], Anna Roujeinikova[1,2,*]

[1] Department of Microbiology, Infection and Immunity Program, Monash Biomedicine Discovery Institute, Monash University, Melbourne, Victoria, Australia;
[2] Department of Biochemistry and Molecular Biology, Monash University, Melbourne, Victoria, Australia;
[3] Monash Micro Imaging, Biomedicine Discovery Institute, Monash University, Melbourne, Victoria, Australia.

SUMMARY   The bacterial flagellar motor is a molecular nanomachine, the assembly and regulation of which requires many accessory proteins. Their identity, structure and function are often discovered through characterisation of mutants with impaired motility. Here, we demonstrate the functional association of the *Helicobacter pylori* peptidoglycan-associated lipoprotein (*Hp*Pal) with the flagellar motor by analysing the motility phenotype of the Δ*pal* mutant, and present the results of the preliminary X-ray crystallographic analysis of its globular C-terminal domain *Hp*Pal-C. Purified *Hp*Pal-C behaved as a dimer in solution. Crystals of *Hp*Pal-C were grown by the hanging drop vapour diffusion method using medium molecular weight polyethylene glycol (PEG) Smear as the precipitating agent. The crystals belong to the primitive orthorhombic space group P1 with unit cell parameters a = 50.7, b = 63.0, c = 75.1 Å. X-ray diffraction data were collected to 1.8 Å resolution on the Australian Synchrotron beamline MX2. Calculation of the Matthews coefficient (V_M=2.24 Å³/Da) and molecular replacement showed that the asymmetric unit contains two protein subunits. This study is an important step towards elucidation of the non-canonical role of *H. pylori* Pal in the regulation, or function of, the flagellar motor.

Keywords   peptidoglycan-associated lipoprotein, bacterial flagellar motor, motility, *Helicobacter pylori*, crystals

1. Introduction

More than 50% of the world's population carry Gram-negative pathogenic bacteria *Helicobacter pylori* in their stomach (*1*). The presence of *H. pylori* has been causatively linked to chronic gastritis and gastric and duodenal ulcers; furthermore, untreated *H. pylori* infections can lead to the development of gastric cancer (*2-4*). In fact, *H. pylori* infections are the main cause of cancer ascribed to infectious agents, accounting for 0.8 million cancer cases in 2018 alone (*5*). In terms of cancer-related deaths, gastric cancer holds the fourth position (*6*).

The pathogenesis of *H. pylori* infection is partly attributed to the secretion of bacterial toxins, cytotoxin-associated gene product A (CagA) and vacuolating cytotoxin A (VacA), which induce a pathological transformation of the epithelial layer (*7-9*). It is not fully understood why the host's immune system is unable to eradicate *H. pylori* and how it manages to persist in the highly acidic stomach lining. What is known is that *H. pylori* produces enzymes that facilitate adaptation to the very low pH of the stomach (*10*), protect against the host's immune system by digesting innate immune peptides (*11*), eliminate reactive oxygen species produced by white blood cells (*12*), or mask outer surface bacterial proteins with sugars (*13*).

It is also well understood that *H. pylori* requires motility in order to colonize the host and to attain full infection level (*14*). *H. pylori* swims through the dense mucous layer in the stomach by means of its flagella and it uses chemotaxis to move into nutrient-rich areas and towards small molecules that its can use to defend itself from elimination by host complement (*14-16*). Cryo-electron tomography studies showed that the molecular nanomachine at the base of the flagellum, the bacterial flagellar motor, is wider and significantly more complex in *H. pylori* compared to

the motors in *Escherichia coli* and *Salmonella* (*17*). The *H. pylori* motor structure appears to be reinforced by a periplasmic scaffold made of proteins (*17*). The exact function of the scaffold is not yet known, but it has been proposed that it may stabilize the force-generating MotA/MotB stator units and support the wider stator ring to produce a larger turning force (*18*). It is also possible that it serves to regulate the stator function, or, perhaps, forms an extension of the stator itself. The flagellar motor is an example of a biological nanomachine that self-assembles from many different proteins; it was hypothesized that the binding energy released upon incorporation of the MotA/MotB complexes into the periplasmic scaffold drives their activation through conformational changes (*19,20*) that open the stator's proton channel.

Recent advances in the field of cryo-electron tomography led to the discoveries of a similarly complex architecture of polar flagellar motors in many other bacteria (*18*). However, progress in establishing the molecular make-up of the discovered periplasmic scaffolds has been slow, partly because identification of additional motor components through bioinformatic analyses alone may be challenging due to gene recombination events. New putative motor components are often discovered by investigating the underlying molecular mechanisms responsible for impaired motility in strains produced by random or targeted mutagenesis. It was recently reported that deletion of the gene encoding peptidoglycan-associated lipoprotein (Pal) in uropathogenic or enterohemorrhagic *E. coli* produced mutants with lower motility as judged by the migration diameter on 0.3% agar plates (*21,22*). Since Pal has never been directly implicated in the function or regulation of the flagella motor, we wished to examine the motility phenotype of the respective *H. pylori* mutant. We assessed the effect of inactivation the *pal* gene in *H. pylori* strain SS1 on migration in semi-solid agar and on linear swimming speed in liquid medium. Having established that mutants swim slower than wild-type (WT) cells, we performed cloning, purification, crystallization and the preliminary X-ray crystallographic analysis of the C-terminal outer membrane protein A (OmpA)-like globular domain of *H. pylori* Pal (*Hp*Pal-C). This is an important step towards elucidation of its role in the regulation, or function of, the flagellar motor.

2. Materials and Methods

2.1. Insertional inactivation of pal in H. pylori strain SS1

SS1 $\Delta pal::kan$ mutant strain was created by replacing the middle part of the *pal* gene (locus tag HPYLSS1_01070) with the *Campylobacter coli* kanamycin resistance gene *aphA3* (encoding aminoglycoside 3'-phosphotransferase, Genbank ID HG515011.2). A DNA fragment containing *aphA3* (795 bp), flanked by *H. pylori* chromosomal DNA sequences corresponding to 200 bp upstream plus the first 100 bp of the *pal* gene at the 5' end, and the last 100 bp plus 200 bp downstream of the *pal* gene at the 3' end, was synthesized and ligated into the pUC18 vector by GenScript (USA). The SS1 $\Delta pal::kan$ mutant was generated by natural transformation method and selection on Columbia blood agar (Oxoid) plates supplemented with 5%(v/v) defibrinated horse blood and an antibiotic mixture comprising 10 μg/mL kanamycin, 10 μg/mL vancomycin, 2.5 U/mL polymyxin B, 5 μg/mL trimethroprim (all antibiotics from Sigma-Aldrich). The mutation was verified by Sanger sequencing.

2.2. Semisolid agar motility assay

Brucella broth plates were prepared with 0.4%(w/v) bacteriological agar (Oxoid), 7%(v/v) fetal bovine serum (Gibco), 40 μg/mL triphenyl tetrazolium chloride (Sigma, UK), and *H. pylori*-selective antibiotics (10 μg/mL vancomycin, 2.5 U/mL polymyxin B, 5 μg/mL trimethroprim, plus 10 μg/mL kanamycin for the $\Delta pal::kan$ mutant). *H. pylori* SS1 WT or mutant strains were cultured overnight in BB10 (Brucella broth (Becton Dickinson) supplemented with 10 μg/mL vancomycin and 10%(v/v) foetal bovine serum (plus 10 μg/mL kanamycin for the mutant) under microaerobic conditions generated using the CampyGen (Oxoid) system. Five μL of the overnight culture adjusted to an OD_{600} nm of 0.74 was inoculated into agar, and the plates were incubated under microaerobic conditions at 37°C for 7 days. The diameter of the migration halos was measured, and the values averaged over 7 biological repeats.

2.3. Measurement of swimming speeds

For optical microscopy filming of bacteria swimming in liquid media, strains were cultured overnight in BB10, inoculated into fresh pre-warmed BB10 to an optical density at 600 nm (OD600) of 0.05 and grown for a further 2–3 hrs. To observe the cells swimming behaviour, 10 μL of the cell suspension was placed in a EVE cell counting slide (EVS-050) and imaged using a Leica DMi8 microscope (Leica Microsystems, Germany) fitted with a Scientific CMOS K8 camera in bright-field mode at 20× magnification. Five 30-sec time-lapse videos (16 frames per second; fields of view picked randomly) were captured for both wild type (WT) and Δpal cultures, in three independent biological replicates for WT and 2 replicates for Δpal. The time-lapse videos were analysed using ImageJ v. 1.53. A total of 66 cells (WT) and 60 cells (Δpal) that swam in linear fashion for at least 0.5 sec were tracked manually using

the MTrack plug-in to allow calculation of the mean straight swimming speed. A two-sample Student's *t*-test was performed to determine statistical significance of the observed swimming speed differences between the WT and Δ*pal::kan* mutant.

2.4. Gene cloning and overexpression

The amino acid sequence of *H. pylori* Pal (Uniprot ID A0A1U9IUR5) was analysed for the presence of signal peptides and disordered regions using the servers SignalP 6.0 (*https://services.healthtech.dtu.dk/services/SignalP-6.0/#6.0*) (*23*) and DISOPRED3 (*http://bioinf.cs.ucl.ac.uk/disopred*) (*24*), respectively. The codon-optimized coding sequence for the C-terminal outer membrane protein A (OmpA)-like globular domain of *H. pylori* Pal (*Hp*Pal-C, amino-acid residues 66-179) was synthesized and ligated into the pET151/D-TOPO vector (Invitrogen) by GenScript (Piscataway, USA) to produce an *Escherichia coli* expression vector that adds an N-terminal His$_6$ tag, V5-epitope and a tobacco etch virus (TEV) protease cleavage site. *E. coli* BL21(DE3) cells were transformed with the expression vector and grown at 37°C in LB medium supplemented with 50 mg/L ampicillin. Overexpression of *Hp*Pal-C was induced with 1 mM isopropyl-*D*-1-thiogalactopyranoside at an OD$_{600}$ of 0.6-0.8, the cells were grown for a further 4 hrs and then harvested by centrifugation at 6,000 g for 15 min.

2.5. Purification and oligomeric state analysis

Recombinant *Hp*Pal-C was purified by following the procedure modified from that described in (*25*). The cell lysate was loaded onto a 5-mL Ni-NTA affinity column (Cytiva) pre-equilibrated with 20 mM Tris-HCl pH 8.0, 500 mM NaCl and 15 mM imidazole. The column was washed with 100 mL of 20 mM Tris-HCl pH 8.0, 500 mM NaCl, 40 mM imidazole and the protein was eluted with the buffer containing 20 mM Tris-HCl pH 8.0, 500 mM NaCl and 500 mM imidazole. TEV was added (Invitrogen), and the sample was dialyzed overnight at 4°C against the buffer containing 20 mM Tris-HCl pH 8.0, 150 mM NaCl, 2 mM DTT, 1% (v/v) glycerol to cleave the tag off, producing the *Hp*Pal-C protein comprising residues 66–179 (the C-terminal domain) of *Hp*Pal plus six additional residues from the TEV cleavage site (GIDPFT). The protease, tag and uncleaved protein were removed by passing the sample through the Ni-NTA column, and the protein was further purified using a HiLoad 16/600 Superdex 75 prep grade gel filtration column (Cytiva) equilibrated with 10 mM Tris-HCl pH 8.0, 150 mM NaCl. Protein concentration was determined using the Bradford assay (*26*), and SDS-PAGE was used to ascertain the degree of protein purity.

The calibration curve for the gel filtration column was established by fitting the retention volumes (V$_R$) and molecular weights (MW) of calibration standards listed in the manufacturer's manual (*https://cdn.cytivalifesciences.com/api/public/content/digi-11217-pdf*) to the equation MW = A × exp(-B × V$_R$) (*27*). The resulting standard curve MW = 957.6 × exp(-0.048 × V$_R$) was used to determine the oligomeric state of *Hp*Pal-C in solution.

2.6. Crystallisation

*Hp*Pal-C was concentrated to 15 mg/mL and subjected to 20-min centrifugation at 17,000 g to remove insoluble particles and aggregates. The crystallization screening was carried out by the sitting-drop vapour-diffusion method using an automated Phoenix crystallization robot (Art Robbins Instruments) and commercial screens LFS, LMB, BCS, MIDAS (Molecular Dimensions), Crystal Screen HT, and PEG/Ion HT (Hampton Research). 100 nL protein solution was combined with an equal volume of reservoir solution and equilibrated against 50 μL reservoir solution in a 96-well Art Robbins CrystalMation Intelli-Plate (Hampton Research). Rod-like crystals appeared after one day in condition B6 of the BCS screen, which contained 25%(w/v) PEG Smear Medium and 100 mM Bicine pH 9.3. Following optimization, larger crystals were produced using drops containing 1 μL protein solution (13.2 mg/mL) mixed with 2 μL reservoir solution (25%(w/v) PEG Smear Medium, 100 mM Bicine pH 8.7) and equilibrated against 500 μL reservoir solution at 293 K.

2.7. X-ray diffraction data collection and processing

For data collection, crystals of *Hp*Pal-C were briefly soaked in a cryoprotectant solution, prepared as the reservoir solution supplemented with 15%(v/v) glycerol, and flash-frozen by plunging in liquid nitrogen. X-ray diffraction data from a cryocooled crystal were collected to 1.8 Å on the MX2 beamline of the Australian Synchrotron. The data were processed and scaled using *XDS* (*28*) and *AIMLESS* (*29*) from the Collaborative Computational Project, Number 4 (*CCP4*) suite (*30*). Data collection and processing statistics are summarized in Table 1.

2.8. Molecular replacement

To identify an appropriate model for molecular replacement, we conducted a sequence-similarity search against the crystal structures deposited in the RCSB Protein Data Bank. The three most similar sequences were those of Pals from *Burkholderia cenocepacia* (PDB ID 5n2c (*31*)), *Burkholderia pseudomallei* (PDB ID 4b5c (*32*)) and *Acinetobacter baumannii* (PDB ID 4g4x). Molecular replacement with these structures

Table 1. Data collection and processing. Values in parentheses correspond to the highest resolution shell

Diffraction source	MX2 beamline, Australian Synchrotron
Wavelength (Å)	0.95
Temperature (K)	100
Detector	Dectris EIGER 16M
Total rotation range (º)	80
Space group	$P2_12_12_1$
a, b, c (Å)	50.7, 63.0, 75.1
α, β, γ (º)	90, 90, 90
Mosaicity (º)	0.05
Resolution range (Å)	48.26-1.79 (1.83–1.79)
Total No. of reflections	69,134 (4.093)
No. of unique reflections	22,855 (1,348)
Completeness (%)	98.6 (98.7)
Multiplicity	3.0
$<I/\sigma(I)>$	8.4 (1.8)
$CC_{1/2}$ (%)	99.7 (80.7)
R_{merge}	0.054 (0.425)

as search models and preliminary refinement were performed using Phaser (*33*) and Phenix (*34*).

3. Results and Discussion

3.1. *H. pylori* SS1 Δ*pal* mutant shows a significant motility defect in semisolid agar

To examine whether *H. pylori* Pal is required for motility, we generated an isogenic Δ*pal* mutant strain lacking functional Pal by replacing the middle part of the gene with the kanamycin resistance gene *aphA3*. We first compared motility of the WT and mutant cells using the semisolid agar plates assay, where a small, set amount of the strain to be tested is stabbed into the thickness of the agar and the diameter of the bacterial migration halo is measured after several days. The ability of *H. pylori* mutants lacking Pal to migrate through semisolid (0.4%) agar was drastically reduced compared to wild type (WT) strain (Figure 1A). We concluded that Pal promotes migration of bacteria on a semisolid agar surface.

3.2. *H. pylori* SS1 Δ*pal* mutants are unable to achieve WT linear swimming speeds in liquid media

We recognise that although the diameter of the halos in soft agar plate assays strongly correlates with migration ability, it is also influenced by the growth rate and chemotaxis artefacts. Therefore, to further characterize the motility phenotype of the *H. pylori* Δ*pal* strain, we filmed bacteria swimming in liquid media (BB10) using bright-field optical microscopy and measured their linear swimming speeds. The mean straight swimming speeds for the WT cells and Δ*pal* mutants were 97 ± 16 µm/sec and 88 ± 13 µm/sec, respectively (Figure 1b). The reduction in the linear swimming speed caused by elimination of Pal was small (9%) but statistically significant ($p < 0.01$). The flagella in *H. pylori* Δ*pal* mutants have normal morphology (*35*). The observed linear speed reduction is therefore likely caused by the reduction in the rotational speed of the flagellar motor. Our observation thus indicates that the loss of the cellular function of *H. pylori* Pal impacts on the generation of force in the flagellar motor.

3.3. Cloning, overexpression, purification and biochemical characterisation of the C-terminal globular domain of *H. pylori* Pal (*Hp*Pal-C)

Bioinformatic analysis of *H. pylori* Pal revealed that is contains a signal peptide and a lipobox recognisable by the signal peptidase II (Figure 2A), identifying it as a lipoprotein. Secondary structure prediction and homology searches suggested that *Hp*Pal contains a C-terminal OmpA-like globular domain (*Hp*Pal-C, residues 66–179) connected to the lipid anchor by a flexible, unstructured tether (19–65). The globular domain *Hp*Pal-C was over-expressed in BL21(DE3) cells from the pET151/D-TOPO vector and purified using Ni-NTA affinity and size exclusion chromatography to > 98% electrophoretic homogeneity based on Coomassie Blue staining of the SDS-PAGE gel (Figure 2B).

It migrated on SDS–PAGE with an apparent molecular weight of ~13.5 kDa, which is close to the value calculated from the amino-acid sequence (13.0 kDa). When subjected to size exclusion chromatography, *Hp*Pal-C eluted as a single symmetrical peak with the retention volume of 72.6 mL (data not shown). Estimation of the particle weight based on the calibration of the size exclusion column using globular proteins of a known mass gave the value of approximately 29.4 kDa, which suggested that *Hp*Pal-C is a dimer in solution under the tested conditions.

3.4. Crystallisation and preliminary crystallographic analysis

Crystals of *Hp*Pal-C (Figure 2C) were obtained using screening by sparse matrix sampling. An X-ray diffraction data set was collected from a single cryo-cooled crystal on beamline MX2 at the Australian Synchrotron (AS) to a resolution of 1.8 Å. Autoindexing of the diffraction data using *XDS* and analysis of axial systematic absences indicated that the crystal belonged to the primitive orthorhombic space group $P2_12_12_1$, with unit-cell parameters a = 50.7, b = 63.0, c = 75.1 Å, α = β = γ = 90°. The average $I/\sigma(I)$ value was 8.4 for all reflections (resolution range 48.3–1.8 Å) and 1.8 in the highest resolution shell (1.83–1.79 Å). The Rmerge value for intensities was 0.054 (0.425 in the highest resolution shell), and these data were 99% complete (99% completeness in the outer shell as well).
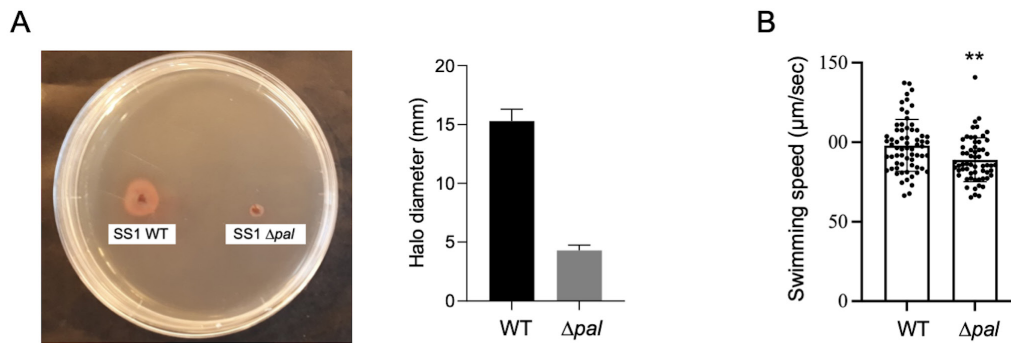
Figure 1. *H. pylori* SS1 Δ*pal* mutant shows motility defects both in semi-solid and liquid media. (A) Soft agar motility assay of *H. pylori* SS1 WT and Δ*pal::kan* mutant with visualisation aided by a colorimetric metabolic activity indicator triphenyl tetrazolium chloride. Brucella broth plates were prepared with 0.4%(w/v) bacteriological agar, 7%(v/v) fetal bovine serum, 40 μg/mL triphenyl tetrazolium chloride, and *H. pylori*-selective antibiotics (10 μg/mL vancomycin, 2.5 U/mL polymyxin B, 5 μg/mL trimethroprim). **(B)** Swimming speeds of *H. pylori* SS1 WT and Δ*pal* in liquid media BB10. For each strain, the speeds of individual cells, the mean value (97 ± 16 μm/sec for WT, 88 ± 13 μm/sec for the mutant) and the standard deviation are shown. **p < 0.01.
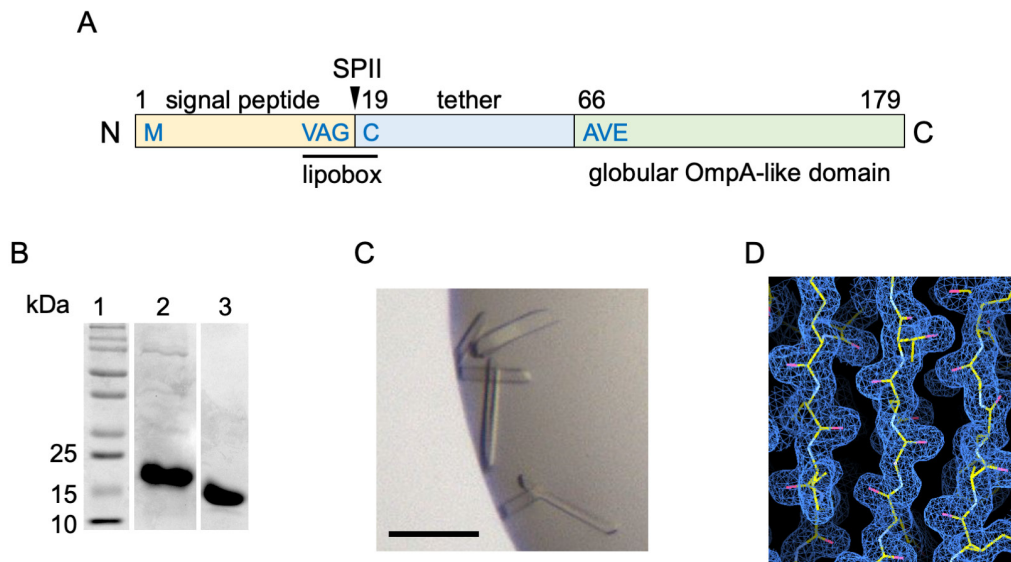

Figure 2. Production and preliminary crystallographic analysis of the C-terminal globular domain of *H. pylori* Pal (*Hp*Pal-C). (A) Schematics of full-length *H. pylori* Pal, showing N-terminal signal peptide, lipobox, site of cleavage by signal peptidase II (SPII), disordered tether and the C-terminal globular OmpA-like domain (residues 66-179) that was produced and crystallised in this study. **(B)** Coomassie Blue-stained 15% SDS-PAGE gel of Ni-NTA purified His-tagged *Hp*Pal-C (lane 2) and *Hp*Pal-C after tag cleavage and gel filtration chromatography (lane 3). **(C)** Crystals of *Hp*Pal-C. Scale bar corresponds to 0.1 mm. **(D)** Representative portion of the electron density map of the molecular replacement solution after preliminary XYZ, B refinement. The contour level is 1 σ.

Calculation of the Matthews coefficient (V_M) (*36*) suggested that the asymmetric unit most likely contains 2 molecules (V_M=2.24 Å³/Da). In agreement with this, a molecular replacement (MR) search, performed using the structures of Pals from *B. cenocepacia*, *B. pseudomallei* and *A. baumannii* as search models, yielded solutions that contained 2 subunits. One round of XYZ, B refinement of the solution based on *A. baumannii* Pal (log likelihood gain function = 291) resulted in the largest decrease of R/Rfree values (to 0.365/0.408) of the three models. Inspection of the electron density map revealed good agreement with the partially refined MR solution (Figure 2D). Exhaustive refinement in Phenix with iterative model rebuilding in Coot (*37*) are in progress.

3.5. Discussion

The canonical Tol-Pal system in the bacterial cell wall comprises the cytoplasmic membrane proteins TolA, TolQ and TolR, the periplasmic protein TolB and the outer membrane protein Pal (*38*). Pal, bound *via* its N-terminal anchor to the outer membrane, and *via* its C-terminal OmpA-like domain to the peptidoglycan, is important for the integrity of the outer membrane. In some bacteria, including *E. coli*, the Tol-Pal system plays an important role in cell division, by promoting the constriction of the outer membrane (*39*) and peptidoglycan restructuring at the septum (*38*).

Although *H. pylori* Pal shares 38% amino acid sequence identity with the well-characterised Pal

component of the *E. coli* Tol-Pal system, *H. pylori* does not have homologs of the inner membrane components of this system (TolA, TolQ or TolR) (*35*). This suggests that *H. pylori* may possess a non-canonical TolB/Pal system that has a different primary function. A previous study of the Δ*pal* (HP1125) mutant of non-motile *H. pylori* strain 26695 (*35*) pointed to a possible association of Pal with the flagellar motor, although the results were not conclusive. However, recent reports of *E. coli pal* mutants with reduced motility in semi-solid agar (*21,22*) also pointed to the possible involvement of Pal in the regulation or function of the flagellar motor. In this study, we performed preliminary X-ray crystallographic analysis of Pal from *H. pylori* and evaluated its requirement for *H. pylori* motility in both liquid and semi-solid media. Under both conditions, inactivation of the *pal* gene produced flagellated cells with reduced motility. These results demonstrate the functional association of *Hp*Pal with the flagellar motor. We note that the motility defects were more prominent in semi-solid agar, and only a modest reduction in the linear swimming speed was observed in liquid medium. Although it remains to be established if *Hp*Pal is an integral component of the periplasmic scaffold of the *H. pylori* flagellar motor, our results suggest that *Hp*Pal plays a novel, non-canonical role by regulating the function of the motor in response to surface contact or increased viscosity. Our observation that, in contrast to other characterised Pals that are monomeric in solution (*40,41*), *Hp*Pal behaves as a dimer, may be related to this different role.

Pals have been studied extensively as potential targets for new therapeutics for several reasons. *i*) In some bacteria, *e.g. Caulobacter crescentus* (*42*), *pal* is essential. *ii*) A fraction of the Pal molecules become exposed on the surface of bacteria, which has been exploited in the design and evaluation of many vaccine candidates (*38,43*). *iii*) In *A. baumannii*, the surface-exposed Pal interacts with host fibronectin (*43*); blocking this interaction with small molecules may offer a new strategy to combat bacterial infections. *iv*) Pal was also shown to be important for production of biofilm (*43*). *v*) In addition, importance of Pal for persister cell formation during antibiotic treatment of *E. coli* has been demonstrated (*44*). *vi*) Furthermore, *E. coli* Pal was shown to be required for the production of the capsular polysaccharide and resistance to serum (*45*). *vii*) Finally, *A. baumannii* Pal was found to contribute to virulence by regulating the twitching motility (*43*). The latter finding about the role of Pal in the type IV pili-mediated motility is particularly interesting because the results of our study suggest that Pal can also regulate flagellar motor-mediated motility, which adds yet another facet to the role of this enigmatic protein. The purification, crystallisation and preliminary X-ray diffraction analysis of recombinant *Hp*Pal-C presented in this study is an important step towards elucidation of the non-canonic *Hp*Pal function and exploration of its therapeutic potential.

In conclusion, *H. pylori* SS1 Δ*pal* mutant strain showed a significant motility defect in semisolid agar. The Δ*pal* mutants were also unable to achieve WT linear swimming speeds in liquid media. Cloning, overexpression, purification and biochemical characterisation of the C-terminal globular domain of *H. pylori* Pal (*Hp*Pal-C) allowed us to perform its preliminary X-ray crystallographic analysis. The outcomes of this work pave the way to future studies aimed at elucidation of the role of *Hp*Pal in the regulation, or function of, the flagellar motor.

References

1. Hooi JKY, Lai WY, Ng WK, Suen MMY, Underwood FE, Tanyingoh D, Malfertheiner P, Graham DY, Wong VWS, Wu JCY, Chan FKL, Sung JJY, Kaplan GG, Ng SC. Global prevalence of *Helicobacter pylori* infection: Systematic review and meta-analysis. Gastroenterology. 2017; 153:420-429.
2. Warren JR, Marshall B. Unidentified curved bacilli on gastric epithelium in active chronic gastritis. Lancet. 1983; 1:1273-1275.
3. The EUROGAST Study Group. An international association between *Helicobacter pylori* infection and gastric cancer. Lancet. 1993; 341:1359-1362.
4. Peek RM Jr, Blaser MJ. *Helicobacter pylori* and gastrointestinal tract adenocarcinomas. Nat Rev Cancer. 2002; 2:28-37.
5. de Martel C, Georges D, Bray F, Ferlay J, Clifford GM. Global burden of cancer attributable to infections in 2018: a worldwide incidence analysis. Lancet Glob Health. 2020; 8:e180-e190.
6. Sung H, Ferlay J, Siegel RL, Laversanne M, Soerjomataram I, Jemal A, Bray F. Global Cancer Statistics 2020: GLOBOCAN estimates of incidence and mortality worldwide for 36 cancers in 185 countries. CA Cancer J Clin. 2021; 71:209-249.
7. Evans DG, Queiroz DM, Mendes EN, Evans DJ Jr. *Helicobacter pylori cagA* status and *s* and *m* alleles of

vacA in isolates from individuals with a variety of *H. pylori*-associated gastric diseases. J Clin Microbiol. 1998; 36:3435-3437.

8. Tohidpour A, Gorrell RJ, Roujeinikova A, Kwok T. The middle fragment of *Helicobacter pylori* CagA induces actin rearrangement and triggers its own uptake into gastric epithelial cells. Toxins (Basel). 2017; 9:237.

9. Roujeinikova A. Phospholipid binding residues of eukaryotic membrane-remodelling F-BAR domain proteins are conserved in *Helicobacter pylori* CagA. BMC Res Notes. 2014; 7:525.

10. Krulwich TA, Sachs G, Padan E. Molecular aspects of bacterial pH sensing and homeostasis. Nat Rev Microbiol. 2011; 9:330-343.

11. Modak JK, Rut W, Wijeyewickrema LC, Pike RN, Drag M, Roujeinikova A. Structural basis for substrate specificity of *Helicobacter pylori* M17 aminopeptidase. Biochimie. 2016; 121:60-71.

12. Stent A, Every AL, Sutton P. *Helicobacter pylori* defense against oxidative attack. Am J Physiol Gastrointest Liver Physiol. 2012; 302:G579-G587.

13. Ud-Din AI, Liu YC, Roujeinikova A. Crystal structure of *Helicobacter pylori* pseudaminic acid biosynthesis N-acetyltransferase PseH: Implications for substrate specificity and catalysis. PLoS One. 2015; 10:e0115634.

14. Hanyu H, Engevik KA, Matthis AL, Ottemann KM, Montrose MH, Aihara E. *Helicobacter pylori* uses the TlpB receptor to sense sites of gastric injury. Infect Immun. 2019; 87:e00202-19.

15. Hu S, Ottemann KM. *Helicobacter pylori* initiates successful gastric colonization by utilizing L-lactate to promote complement resistance. Nat Commun. 2023; 14:1695.

16. Machuca MA, Johnson KS, Liu YC, Steer DL, Ottemann KM, Roujeinikova A. *Helicobacter pylori* chemoreceptor TlpC mediates chemotaxis to lactate. Sci Rep. 2017; 7:14089.

17. Qin Z, Lin WT, Zhu S, Franco AT, Liu J. Imaging the motility and chemotaxis machineries in *Helicobacter pylori* by cryo-electron tomography. J Bacteriol. 2017; 199:e00695-16.

18. Zhou X, Roujeinikova A. The structure, composition, and role of periplasmic stator scaffolds in polar bacterial flagellar motors. Front Microbiol. 2021; 12:639490.

19. Tachiyama S, Chan KL, Liu X, Hathroubi S, Peterson B, Khan MF, Ottemann KM, Liu J, Roujeinikova A. The flagellar motor protein FliL forms a scaffold of circumferentially positioned rings required for stator activation. Proc Natl Acad Sci USA. 2022; 119:e2118401119.

20. Reboul CF, Andrews DA, Nahar MF, Buckle AM, Roujeinikova A. Crystallographic and molecular dynamics analysis of loop motions unmasking the peptidoglycan-binding site in stator protein MotB of flagellar motor. PLoS One. 2011; 6:e18981.

21. Hirakawa H, Suzue K, Kurabayashi K, Tomita H. The Tol-Pal system of uropathogenic *Escherichia coli* is responsible for optimal internalization into and aggregation within bladder epithelial cells, colonization of the urinary tract of mice, and bacterial motility. Front Microbiol. 2019; 10:1827.

22. Hirakawa H, Suzue K, Takita A, Awazu C, Kurushima J, Tomita H. Roles of the Tol-Pal system in the Type III secretion system and flagella-mediated virulence in enterohemorrhagic *Escherichia coli*. Sci Rep. 2020;

23. Teufel F, Almagro Armenteros JJ, Johansen AR, Gíslason MH, Pihl SI, Tsirigos KD, Winther O, Brunak S, von Heijne G, Nielsen H. SignalP 6.0 predicts all five types of signal peptides using protein language models. Nat Biotechnol. 2022; 40:1023-1025.

24. Jones DT, Cozzetto D. DISOPRED3: precise disordered region predictions with annotated protein-binding activity. Bioinformatics. 2015; 31:857-863.

25. Woon AP, Tohidpour A, Alonso H, Saijo-Hamano Y, Kwok T, Roujeinikova A. Conformational analysis of isolated domains of *Helicobacter pylori* CagA. PLoS One. 2013; 8:e79367.

26. Bradford MM. A rapid and sensitive method for the quantitation of microgram quantities of protein utilizing the principle of protein-dye binding. Anal Biochem. 1976; 72:248-254.

27. Dawkins JV. Size Exclusion Chromatography. In: Comprehensive Polymer Science and Supplements (Allen G., Bevington JC, eds.). Pergamon, 1989, pp. 231-238.

28. Kabsch W. *XDS.* Acta Crystallogr D Biol Crystallogr. 2010; 66:125-132.

29. Evans PR, Murshudov GN. How good are my data and what is the resolution? Acta Crystallogr D Biol Crystallogr. 2013; 69:1204-1214.

30. Winn MD, Ballard CC, Cowtan KD, *et al.* Overview of the CCP4 suite and current developments. Acta Crystallogr D Biol Crystallogr. 2011; 67:235-242.

31. Capelli R, Matterazzo E, Amabili M, Peri C, Gori A, Gagni P, Chiari M, Lertmemongkolchai G, Cretich M, Bolognesi M, Colombo G, Gourlay LJ. Designing probes for immunodiagnostics: Structural insights into an epitope targeting *Burkholderi*a infections. ACS Infect Dis. 2017; 3:736-743.

32. Gourlay LJ, Peri C, Ferrer-Navarro M, *et al.* Exploiting the *Burkholderia pseudomallei* acute phase antigen BPSL2765 for structure-based epitope discovery/design in structural vaccinology. Chem Biol. 2013; 20:1147-1156.

33. McCoy AJ, Grosse-Kunstleve RW, Adams PD, Winn MD, Storoni LC, Read RJ. Phaser crystallographic software. J Appl Crystallogr. 2007; 40:658-674.

34. Liebschner D, Afonine PV, Baker ML, *et al.* Macromolecular structure determination using X-rays, neutrons and electrons: Recent developments in Phenix. Acta Crystallogr D Struct Biol. 2019; 75:861-877.

35. Turner L, Praszkier J, Hutton ML, Steer D, Ramm G, Kaparakis-Liaskos M, Ferrero RL. Increased outer membrane vesicle formation in a *Helicobacter pylori tolB* mutant. Helicobacter. 2015; 20:269-283.

36. Matthews BW. Solvent content of protein crystals. J Mol Biol. 1968; 33:491-497.

37. Emsley P, Cowtan K. Coot: Model-building tools for molecular graphics. Acta Crystallogr D Biol Crystallogr. 2004; 60:2126-2132.

38. Szczepaniak J, Press C, Kleanthous C. The multifarious roles of Tol-Pal in Gram-negative bacteria. FEMS Microbiol Rev. 2020; 44:490-506.

39. Petiti M, Serrano B, Faure L, Lloubes R, Mignot T, Duché D. Tol energy-driven localization of pal and anchoring to the peptidoglycan promote outer-membrane constriction. J Mol Biol. 2019; 431:3275-3288.

40. Parsons LM, Lin F, Orban J. Peptidoglycan recognition by Pal, an outer membrane lipoprotein. Biochemistry. 2006; 45:2122-2128.

41. Dennehy R, Romano M, Ruggiero A, Mohamed

YF, Dignam SL, Mujica Troncoso C, Callaghan M, Valvano MA, Berisio R, McClean S. The *Burkholderia cenocepacia* peptidoglycan-associated lipoprotein is involved in epithelial cell attachment and elicitation of inflammation. Cell Microbiol. 2017; 19:e12691.

42. Yeh YC, Comolli LR, Downing KH, Shapiro L, McAdams HH. The *Caulobacter* Tol-Pal complex is essential for outer membrane integrity and the positioning of a polar localization factor. J Bacteriol. 2010; 192:4847-4858.

43. Solanki V, Tiwari M, Tiwari V. Investigation of Peptidoglycan-Associated Lipoprotein of *Acinetobacter baumannii* and Its Interaction with Fibronectin to Find Its Therapeutic Potential. Infect Immun. 2023; 91:e0002323.

44. Sulaiman JE, Hao C, Lam H. Specific enrichment and proteomics analysis of *Escherichia coli* persisters from rifampin pretreatment. J Proteome Res. 2018; 17:3984-3996.

45. Diao J, Bouwman C, Yan D, Kang J, Katakam AK, Liu P, Pantua H, Abbas AR, Nickerson NN, Austin C, Reichelt M, Sandoval W, Xu M, Whitfield C, Kapadia SB. Peptidoglycan Association of murein lipoprotein is required for KpsD-Dependent group 2 capsular polysaccharide expression and serum resistance in a uropathogenic *Escherichia coli* isolate. mBio. 2017; 8:e00603-17.

*Address correspondence to:
Anna Roujeinikova, Department of Microbiology, Infection and Immunity Program, Monash Biomedicine Discovery Institute; Department of Biochemistry and Molecular Biology, Monash University, Melbourne, Victoria, Australia.
E-mail: anna.roujeinikova@monash.edu